

This is a repository copy of *Comparative Analysis and Optimization of Novel Pulse Injection Sensorless Drive Methods for Fault-Tolerant DC Vernier Reluctance Machine*.

White Rose Research Online URL for this paper:

<https://eprints.whiterose.ac.uk/192644/>

Version: Accepted Version

---

**Article:**

Wang, Weiyu, Zhao, Xing [orcid.org/0000-0003-4000-0446](https://orcid.org/0000-0003-4000-0446) and Niu, Shuangxia (2022) Comparative Analysis and Optimization of Novel Pulse Injection Sensorless Drive Methods for Fault-Tolerant DC Vernier Reluctance Machine. IEEE Transactions on Power Electronics. ISSN 0885-8993

<https://doi.org/10.1109/TPEL.2022.3182054>

---

**Reuse**

Items deposited in White Rose Research Online are protected by copyright, with all rights reserved unless indicated otherwise. They may be downloaded and/or printed for private study, or other acts as permitted by national copyright laws. The publisher or other rights holders may allow further reproduction and re-use of the full text version. This is indicated by the licence information on the White Rose Research Online record for the item.

**Takedown**

If you consider content in White Rose Research Online to be in breach of UK law, please notify us by emailing [eprints@whiterose.ac.uk](mailto:eprints@whiterose.ac.uk) including the URL of the record and the reason for the withdrawal request.

# Comparative Analysis and Optimization of Novel Pulse Injection Sensorless Drive Methods for Fault-Tolerant DC Vernier Reluctance Machine

Weiyu Wang, Xing Zhao, *Member, IEEE*, Shuangxia Niu, *Senior Member, IEEE*, W.N. Fu

**Abstract**—Multiphase DC-Excited Vernier reluctance machine (DC-VRM) exhibits the merits of robust structure, small torque ripple and good fault-tolerant ability. Developing advanced sensorless drive methods can further promote its application in the safety-critical system. In this paper, pulse injection sensorless drive methods are optimized in a 6-phase DC-VRM parallel H-bridge drive system to strengthen their acceleration performance and fault-tolerant ability. The acceleration performance studied in this article corresponds to the acceleration speed during the startup stage. By the full-phase alternative pulse injection method (APIM), each phase can be excited independently to avoid mutual inductance influence on position estimation, but this method suffers from a long communication delay and relatively poor acceleration performance. A reduced-phase alternative pulse injection method (APIM) can reduce detection time, but the lack of detected phase may influence position estimation accuracy and fault-tolerant ability. To solve these problems, a novel vertical-axis synchronous pulse injection method (SPIM) is proposed and compared with previous methods in this paper. The key is to inject detection pulses into vertical-axis phases simultaneously, thus reducing the detection time and improving the torque generation. It is proved that the influence of mutual inductance on position estimation can be ignored, and the detection accuracy and acceleration performance can be improved without deterioration of fault-tolerant ability.

**Index Terms**—DC-excited vernier reluctance machine (DC-VRM), sensorless drive, vertical-axis synchronous pulse injection.

## I. INTRODUCTION

With an increasing emphasis on environmental protection and energy-saving, the research on transportation electrification shows an upward trend [1-2]. Non-permanent magnets doubly salient reluctance machines with robust structure and harsh environment adaption have attracted a lot of attention [3-4]. Switched reluctance machine (SRM) suffers from large torque ripple and noises because of half-cycle conduction [5]. Doubly-fed doubly salient machine (DF-DSM) can be operated in the

This work was supported by the National Natural Science Foundation of China under Project 52077187 and in part by the Research Grant Council of the Hong Kong Government under Project PolyU 152143/18E and PolyU 152109/20E. (*Corresponding author: Shuangxia Niu*)

Weiyu Wang and Shuangxia Niu are with the Department of Electrical Engineering, The Hong Kong Polytechnic University, Hong Kong. (e-mail: weiyu.wang@connect.polyu.hk; cesxniu@polyu.edu.hk)

Xing Zhao is with the Department of Electronic Engineering, University of York, YO10 5DD York, U.K. (e-mail: xing.zhao@york.ac.uk;)

W.N. Fu is with Shenzhen Institutes of Advanced Technology, Chinese Academy of Sciences, China (e-mail: wn.fu@siat.ac.cn)

whole electrical period, but the torque ripple is still unsatisfied due to the unbalanced magnetic distribution and rich even-order flux harmonics [6]. Illustrated by the emerging flux modulation theory [7-8], a new type of DC-excited Vernier reluctance machine (DC-VRM) exhibits the merits of small torque ripple and minimum cogging torque [9-10].

Multiphase fault-tolerant machine with the parallel drive is widely applied in aerospace applications and electrical propulsion systems [11-12]. By eliminating vulnerable position sensors, system reliability can be further improved by sensorless drive. The high-speed sensorless drive has been relatively mature [13-16], while the detected signal has a low signal-to-noise ratio at zero or low-speed range. For doubly salient reluctance machine low-speed sensorless drive, modulation method [17-18], sense coil method [19-20], current waveform method [21-22] and pulse injection method [23-30] are typical strategies. In the modulation method, by injecting a high-frequency detection signal into the idle phase through an oscillator, the modulated signal is detected by the demodulation circuit, and a switching circuit is required [17-18]. In the sense coil method [19-20], the parallel sense coils are embedded in the slots in reverse series to minimize the mutual inductance coupling. Full-cycle position detection without a switch circuit can be achieved, but this method also requires additional excitation sources and detection circuits.

Without additional hardware, the current waveform method detects the current slop in the current chopping control process and combines the incremental inductance model to estimate rotor position [21-22]. However, with the increase in speed, the number of current chopping waves decreases, so the position detection accuracy is hard to be guaranteed. In addition, the saturation effect of the magnetic circuit needs to be considered, and the machine parameters measurement or fitting is necessary [22]. The pulse injection method does not require *prior* knowledge of the machine parameters, only applies narrow detection pulses injected into the idle phase to detect the inductance indirectly. As the resultant current amplitudes are small, the saturation effect can be ignored to simplify the calculation. Combining the methods of the inductance Fourier model [23], inductance linearity characteristics [24], inductance threshold comparison [25] or inductance vectors [26], the conduction phase can be decided.

However, due to the half-cycle conduction principle of SRM, detection pulses are injected into the idle phase, thereby negative torque is produced, and full-cycle inductance detection

## IEEE POWER ELECTRONICS REGULAR PAPER/LETTER/CORRESPONDENCE

cannot be realized. For DF-DSM, the detection pulses are injected in the time interval between consecutive acceleration pulses [27], thereby full-cycle inductance detection can be acquired. While the communication delay is inevitable because of the discrete detection. To ease this issue, reducing detection time is a potential strategy [28-30]. According to the present conduction state, a single detection pulse is injected, and its resultant current amplitude is compared with that of the acceleration current consuming the same time to determine whether the rotor has reached the next sector [28]. Similarly, a method based on three-phase pulse injection is proposed that the conduction phase is determined by comparing the resultant current amplitudes of parallel phases [29]. Unfortunately, these methods highly depend on the present conduction state and lack fault-tolerant ability. In [30], a two-step, three-phase pulse injection method is proposed to balance the performance.

Mutual inductances between armature windings are not considered in the above DF-DSM sensorless drive methods but cannot be overlooked in DC-VRM sensorless drives. In this paper, optimized sensorless drive methods are performed in a six-phase DC-VRM with a parallel H-bridge converter drive to achieve a solution that combines sensorless merits, low torque ripple and high tracking performance. Also, the fault-tolerant ability is provided not only for open circuit fault but also for current sampling fault. First, by the full-phase alternative pulse injection method (full-phase APIM), mutual inductance influence on position estimation can be avoided. Then, the inherent communication delay is decreased by the reduced-phase alternative pulse injection method (reduced-phase APIM), but the detection accuracy and reliability are traded off. To solve these problems, a novel vertical-axis synchronous pulse injection method (vertical-axis SPIM) is proposed. The key is to inject detection pulses into the stator side vertical-axis phases simultaneously to shorten detection time and avoid the inductance detection bias fundamentally. Moreover, the mutual inductance between the vertical-axis phases is slight and shows an evitable influence on position estimation. A solution that combines accurate position detection, high acceleration performance and strong fault-tolerant ability can be achieved.

This paper is arranged as follows. In Section II, the six-phase DC-VRM mathematical model and the inductance characteristics, are introduced. In Section III, full-phase APIM, as well as indicators influence acceleration performance are illustrated. In Section IV, reduced-phase APIMs are discussed. In Section V, the proposed vertical-axis SPIM is analyzed. In Section VI, a fault diagnosis for fault-tolerant operation is proposed. In Section VII, a test bench is built, and experimental results are shown. Finally, some conclusions are drawn.

## II. CONFIGURATION OF SIX-PHASE DC-VRM

### A. H-Bridge-Converter based Sensorless Drive System

The structure of the six-phase DC-VRM to be studied is provided in Fig. 1(a). The DC field coils are wound on each stator tooth, and the directions of two adjacent DC field coils are opposite. All the DC field coils are connected in series to form one single DC field winding. Six AC armature coils are

wound on each stator tooth as well. A pair of vertical-axis phases are defined as two phases in which the wound stator teeth are vertical in space. For example, phase A and phase D are a pair of vertical-axis phases.

The parallel H-bridge drive configuration is shown in Fig. 1(b). The advantages of the parallel H-bridge converter based sensorless DC-VRM drive system can be summarized as

- (1) Using a parallel H-bridge converter allows each phase to be independently excited, thus the detection pulses can be flexibly regulated to improve acceleration performance.
- (2) The H-bridge drive structure shows a significant advantage in fault-tolerant to improve system reliability.
- (3) This drive system keeps the complementary electromagnetic characteristic of six-phase DC-VRM in reducing torque ripple.

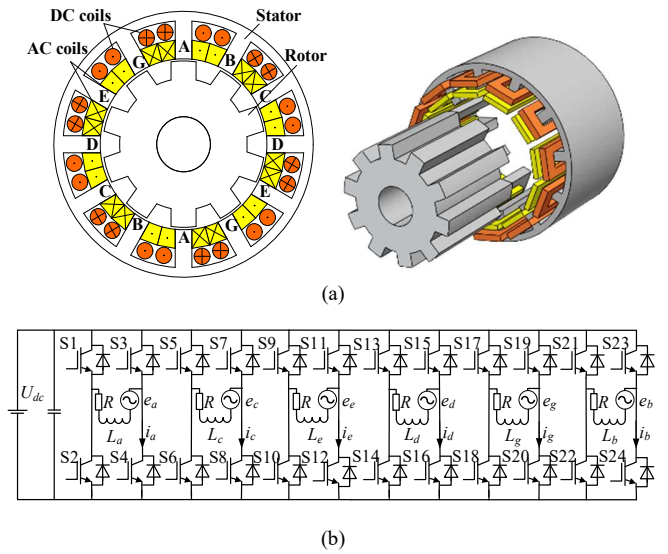


Fig. 1. (a) Structure of six-phase DC-VRM. (b) Parallel H-bridge converter

### B. Mathematical Model

The current and inductance equations can be expressed as

$$I = [i_a \ i_b \ i_c \ i_d \ i_e \ i_g \ i_f]^T \quad (1)$$

$$L = \begin{bmatrix} L_a & L_{ab} & L_{ac} & L_{ad} & L_{ae} & L_{ag} & L_{af} \\ L_{ab} & L_b & L_{bc} & L_{bd} & L_{be} & L_{bg} & L_{bf} \\ L_{ac} & L_{bc} & L_c & L_{cd} & L_{ce} & L_{cg} & L_{cf} \\ L_{ad} & L_{bd} & L_{cd} & L_d & L_{de} & L_{dg} & L_{df} \\ L_{ae} & L_{be} & L_{ce} & L_{de} & L_e & L_{eg} & L_{ef} \\ L_{ag} & L_{bg} & L_{cg} & L_{dg} & L_{eg} & L_g & L_{gf} \\ L_{af} & L_{bf} & L_{cf} & L_{df} & L_{ef} & L_{gf} & L_f \end{bmatrix} \quad (2)$$

where  $I$  is the current matrix,  $i_a, i_b, i_c, i_d, i_e$  and  $i_g$  are the phase currents,  $i_f$  is the field current,  $L$  is the inductance matrix,  $L_{af}, L_{bf}, L_{cf}, L_{df}, L_{ef}$  and  $L_{gf}$  are the mutual inductances between armature windings and the field winding,  $L_a, L_b, L_c, L_d, L_e$  and  $L_g$  are the phase self-inductances,  $L_{ab}, L_{ac}, L_{ad}, L_{ae}, L_{ag}, L_{bc}, L_{bd}, L_{be}, L_{bg}, L_{cd}, L_{ce}, L_{cg}, L_{de}, L_{dg}$  and  $L_{eg}$  are the mutual inductances between armature windings,  $L_f$  is the self-inductance of the field winding. Taking phase A as an example, the torque components under current excitation can be expanded as

$$T_a = i_a i_f \frac{dL_{af}}{d\theta} + \frac{1}{2} i_a^2 \frac{dL_a}{d\theta} + \frac{1}{2} i_f^2 \frac{dL_f}{d\theta} \quad (3)$$

where  $T_a$  is the total torque, and  $\theta$  is the electrical angle. The first term of equation (3) is the major component of the excitation torque produced by the mutual inductance between DC field winding and the AC winding. The second term is the reluctance torque produced by variation of self-inductance. As bipolar current excitation, the average reluctance torque in the whole electrical period is zero. The third term is the cogging torque produced by DC field winding. As  $L_f$  keeps constant in the whole electrical period, the cogging torque can be neglected.

### C. Conduction Model

According to the principle of six-phase DC-VRM, conventional six states conduction is adopted, and the current chopping control is applied as the current regulator. As illustrated in equation (3), the conduction phases of the DC-VRM are determined by the mutual inductance between field winding and armature windings which can be found in Fig. 2. The positive and negative direction currents flow during the rising stage and falling stage of the mutual inductance between the field winding and armature windings, respectively. This trapezoidal inductance feature can effectively avoid the direct current jump from positive to negative and reduce the torque ripples during commutation.

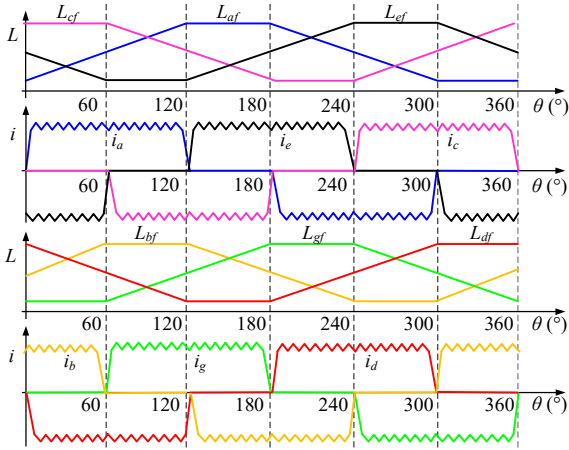


Fig. 2. Conduction mode of six-phase DC-VRM.

### C. Self-inductance Characteristics

In the self-inductance model of six-phase DC-VRM shown in Fig. 3, the amplitudes of each phase are equal, and the phase differences between adjacent phases are  $60^\circ$ .  $0^\circ$  is defined as the position where the self-inductance of phase A starts to rise. Based on the conduction mode, one electrical period can be divided into six sectors through inductance intersections. Three inductance intersections exist at the sector junction. In these intersections, the intersections composed of vertical-axis inductance curves, differed by  $180^\circ$ , are defined as main intersections, and the other two intersections are defined as assist intersections. Also, two middle intersections are in the middle of the sector range.

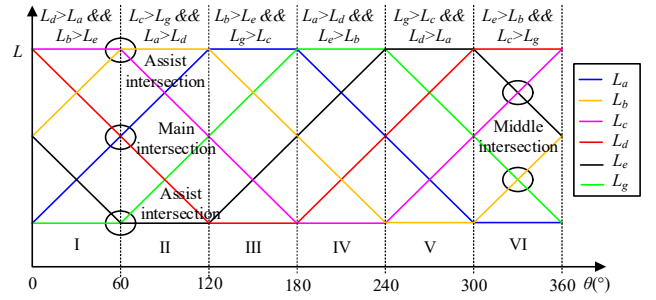


Fig. 3. Self-inductances and inductance intersections.

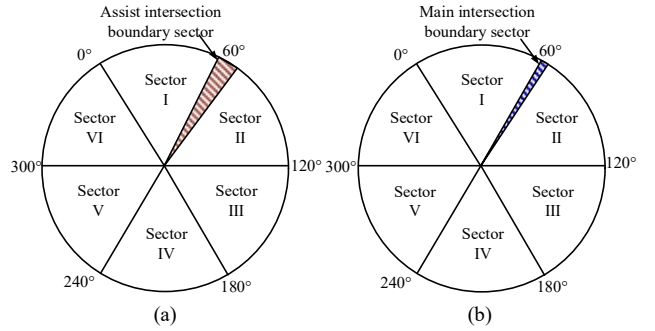


Fig. 4. Boundary sector division. (a) Assist intersection. (b) Main intersection.

For the inductance detection-based position estimation, the inductance amplitudes near the intersections are very close, which makes it difficult to guarantee the sector estimation accuracy by comparing inductance amplitudes. So, a boundary sector exits at the sector junction, which may lead to a poor sector estimation accuracy. The boundary sector ranges produced by the assist intersection and the main intersection are shown in Fig. 4(a) and Fig. 4(b), respectively. A smaller boundary can be acquired by the main intersection-based sector division. That is because the slopes of the inductance curves around the main intersections are obvious, thereby the changes in inductance amplitudes are easily detected, leading to a smaller boundary sector. On the contrary, around assist intersections, the slopes of the inductance curves are not obvious and correspond to a larger boundary sector. So, the inductances detected around the main intersection point are more reliable compared with the assist intersection. In sensorless drive, sector estimation can first rely on main intersections because of a smaller boundary sector. Once the detected information is wrong or missed at the main intersections, the assist intersections can be introduced to provide fault-tolerant ability.

### D. Mutual-inductance Characteristics

The finite element analysis results of flux distributions when phase A is excited at two typical positions  $\alpha$  and  $\beta$  are shown in Fig. 5(a) and Fig. 5(b), respectively. It is noticeable that obvious mutual coupling exists between armature windings. Among them, the mutual inductance between vertical-axis phases A and D is relatively small. That is because when phase A is in a completely aligned position, phase D is in a completely unaligned position. Meanwhile, as can be found in Fig. 5(b), the

meshing trends of the rotor teeth and the stator teeth of vertical-axis phases are opposite. Therefore, the magnetic resistance between vertical-axis phases is large, and the mutual inductance coupling is slight. The mutual inductance can be found in Fig. 6. The fluctuation of  $L_{ad}$  is small in the whole electrical period.

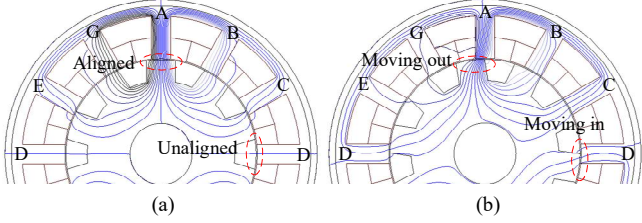


Fig. 5. Flux distributions. (a) Position  $\alpha$ . (b) Position  $\beta$ .

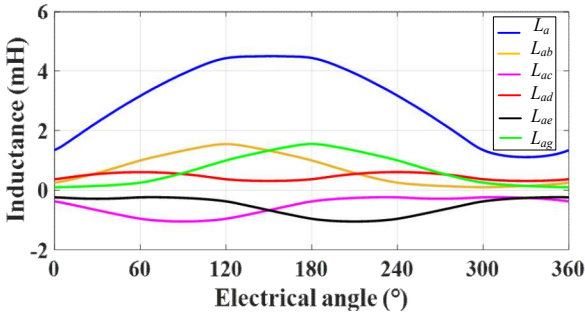


Fig. 6. Inductance curves.

### III. FULL-PHASE ALTERNATIVE PULSE INJECTION METHOD

#### A. Pulse Injection-based Inductance Detection

Fig. 7(a) shows the equivalent circuit during pulse injection in phase A. A short detection voltage pulse is injected by switching on power transistors S1 and S4.  $i_a$  increases sharply during this stage. When the detection pulse injection is finished, the peak point value of  $i_a$  is recorded as  $I_a$ . Meanwhile, S1 and S4 are switched off to enter the demagnetization process which is shown in Fig. 7(b). In this process,  $i_a$  decreases to 0.

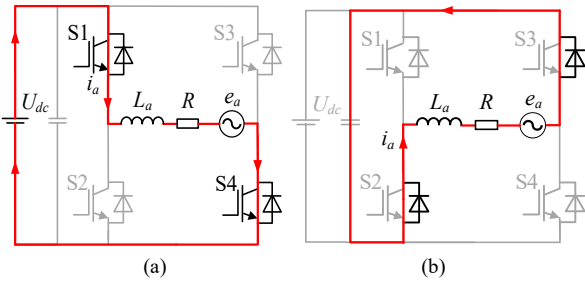


Fig. 7. Equivalent circuit. (a) Pulse injection. (b) Demagnetization.

From Fig. 7(a), The equivalent voltage equation for phase A under pulse injection can be described as

$$U_{dc} = L_a \frac{di_a}{dt} + i_a \frac{dL_a}{d\theta} \omega + i_a R \quad (4)$$

where  $\omega$  is the rotor angular velocity. In the initial detection and acceleration stage,  $\omega$  is zero or quite small, back-EMF can be ignored. In addition, the detection pulse duration is short, and the resultant current amplitude is small, the voltage drop on the winding can also be neglected. As the detection pulse has a short duration, it can be considered that the phase winding current rises linearly during this period. The measured self-inductance equation can be expressed as (5).

$$L_a = \frac{U_{dc} \Delta t}{I_a} \quad (5)$$

where  $\Delta t$  is the detection pulse width. The sector information and the conduction phases can be decided by comparing the self-inductances. The relation can be found in Table I.

TABLE I  
RELATION BETWEEN ELECTRICAL ANGLE, SELF-INDUCTANCES, CONDUCTION PHASES AND ROTOR SECTOR

$\theta$ ( $^\circ$ )	Inductance relation	Conduction phases	Sector
0-60	$L_d > L_a \& \& L_b > L_e$	A, D, B, E	I
60-120	$L_c > L_g \& \& L_a > L_d$	A, D, C, G	II
120-180	$L_b > L_e \& \& L_g > L_c$	B, E, C, G	III
180-240	$L_a > L_d \& \& L_e > L_b$	A, D, B, E	IV
240-300	$L_g > L_c \& \& L_d > L_a$	A, D, C, G	V
300-360	$L_e > L_b \& \& L_c > L_g$	B, E, C, G	VI

#### B. Full-phase Alternative Pulse Injection Method

As shown in Fig. 8, to avoid the mutual inductance influence on position estimation, the detection pulses are injected alternatively. Only one detection phase conducts at the same time, thus the peak current sampling is not affected by mutual inductance. An operation cycle is defined as the period from  $t_1$  to  $t_5$  that consists of alternative detection pulses and acceleration pulses. This method is essentially a discrete sampling of the rotor position. First, the detection pulse sequence is injected during the period from  $t_1$  to  $t_2$ , and the resultant currents are registered. After full phases are detected, the rotor position can be estimated between  $t_2$  and  $t_3$ . Then the conduction phases are determined, and further acceleration pulses are injected during the period from  $t_3$  to  $t_4$ . After each phase completes the demagnetization between  $t_4$  and  $t_5$ , a new round of detection pulses is injected from  $t_5$ .

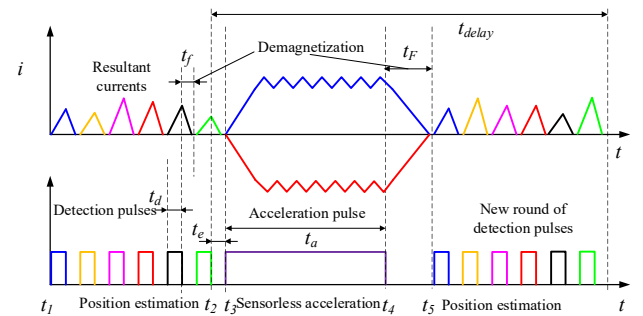


Fig. 8. Schematic diagram of full-phase APIM.

### C. The Indicators that Affect Acceleration Performance

Since full inductance intersections can be detected, when facing current sampling missing or out of reasonable range, assist intersections can be introduced for position estimation to guarantee fault-tolerant ability. While during the acceleration process, since the position information is sampled discretely, the interval of position update leads to a potential commutation delay  $t_{delay}$ , which can be expressed as

$$t_e = t_3 - t_2 \leq t_{delay} \leq t_5 - t_1 + t_3 - t_2 = nt_d + (n-1)t_f + 2t_e + t_a + t_F \quad (6)$$

where  $t_e$  is estimation time,  $n$  is the number of detected phases,  $t_d$  is the width of detection pulse,  $t_f$  is the demagnetization time of detection pulse,  $t_a$  is the width of acceleration pulse,  $t_F$  is the demagnetization time of acceleration pulse. Under a certain pulse width of detection pulse and acceleration pulse,  $t_{delay}$  depends on  $n$ . This kind of commutation delay will cause the lag of the commutation angle  $\theta_{offset}$  or even commutation errors.

$$\theta_{offset} = \omega t_{delay} \quad (7)$$

As  $\theta_{offset}$  exits, the torque generation is constrained, thus limiting the increase of rotor speed. Further, the duty cycle  $\gamma$  that contributes to torque generation is mainly generated by the acceleration pulses, which is defined as

$$\gamma = \frac{t_5 - t_3}{t_5 - t_1} = \frac{t_a + t_F}{nt_d + (n-1)t_f + t_e + t_a + t_F} \quad (8)$$

It is clear to see that the increase of detection time may lead to a decrease in  $\gamma$ , thus constraining torque production.

## IV. REDUCED-PHASE ALTERNATIVE PULSE INJECTION METHOD

In this 6-phase DC-VRM, redundant inductance intersections exist at the sector junction. As one intersection is enough to distinguish sectors, reduced-phase APIM is a potential strategy to reduce  $t_{delay}$  and increase  $\gamma$ . Five-phase APIM, four-phase APIM and three-phase APIM are potential methods. But as  $n$  decreases, when facing the failure of current sensor sampling, reliable sector judgment is hard to be guaranteed. Meanwhile, due to the lack of main intersections, sector judgments must rely on assist intersections, thus leading to a larger boundary sector and a reduction of fault-tolerant ability. How to balance these indicators is a problem that needs to be discussed.

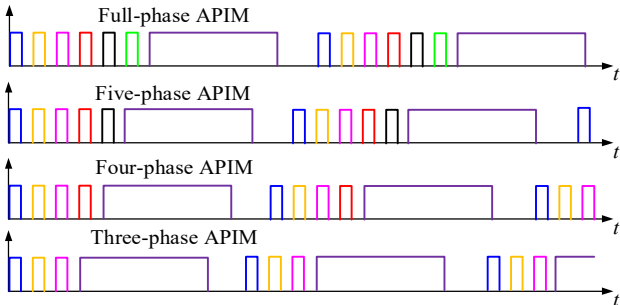


Fig. 9. Schematic diagram of reduced-phases APIM.

### A. Five-phase Alternative Pulse Injection Method

When the sampling of any phase is missing or wrong, the remained inductance intersections can still make the sector estimation. This character confirms the fault-tolerant ability of full-phase APIM. The schematic diagram of potential reduced-phase APIM is shown in Fig. 9.

### B. Four-phase Alternative Pulse Injection Method

As shown in Fig. 10(a), four-phase APIM can be designed that the lacks two phases are on the vertical axis, thereby four main intersections remain. Otherwise, as shown in Fig. 10(b) and Fig. 10(c), only two main intersections remain, accordingly more assist intersections should be introduced for position estimation.

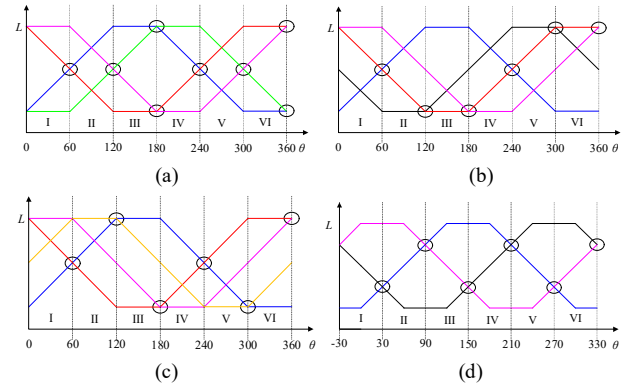


Fig. 10. Reduced-phase APIM. (a) Four-phase case 1. (b) Four-phase case 2. (c) Four-phase case 3. (d) Three-phase.

### C. Three-phase Alternative Pulse Injection Method

For three-phase APIM, the interval of phases should be one-third electrical angle period to achieve a balance sector division. For example, phases A, C and E with  $120^\circ$  intervals are designed as the detection phases to inject the detection pulses, while the other phase B, D and G only inject acceleration pulses. As shown in Fig. 10(d), it is noticeable that this sector division is accompanied by a commutation offset of  $30^\circ$ . That is because all the intersections in this situation are middle intersections. As the existing communication offset, the torque generation is constrained. If  $n$  is less than three, the inductances will be insufficient to make a sector judgment with necessary sector division accuracy by inductance comparison. The reduced-phase APIMs are compared in Table II.  $n_{main}$  is the number of main intersections,  $n_{assist}$  is the number of assist intersections and  $n_{mid}$  is the number of middle intersections.

TABLE II  
COMPARISON OF REDUCED-PHASE APIM

$n$	$n_{main}$	$n_{assist}$	$n_{mid}$	$t_{delay}$	$\gamma$	Fault-tolerant
5	4	8	8	Large	Small	Strong
4 (case 1)	4	2	4	Middle	Middle	Middle
4 (case 2)	2	4	4	Middle	Middle	Middle
4 (case 3)	2	4	4	Middle	Middle	Middle
3	0	0	6	Small	Large	Weak

Reduced-phase APIM has an obvious effect on reducing  $t_{delay}$  and increasing  $\gamma$ , thus improving acceleration performance. It also proves the fault-tolerant ability when facing the current sampling fault. While with the decreasing of detected phases, the absence of inductance intersections may deprive the fault-tolerant ability and detection accuracy. Considering the above reduced-phase APIMs comprehensively, four-phase APIM case 1 shows a balance performance.

## V. VERTICAL-AXIS SYNCHRONOUS PULSE INJECTION METHOD

In this chapter, a novel vertical-axis SPIM is proposed that the detection pulses are injected into vertical-axis phases simultaneously to halve the detection time. It can be proved that the mutual inductance influence on position estimation at the main intersection can be ignored. And the inductance sampling bias caused by APIM can be avoided fundamentally at the main intersection. This method not only has the merit of high fault-tolerant ability but also improves both detection accuracy and acceleration performance at the same time.

### A. Vertical-axis Synchronous Pulse Injection Method

The design principle of vertical-axis SPIM can be illustrated as that the main intersections are composed of vertical-axis phases, and the mutual inductance coupling between them is slight. In addition, the detected inductances of vertical-axis phases are sampled simultaneously, so no detection phase bias exists at the main intersections, which fundamentally avoids the detection error caused by APIM. The equivalent circuit and the schematic diagram of the proposed method are shown in Fig. 11 and Fig. 12, respectively.

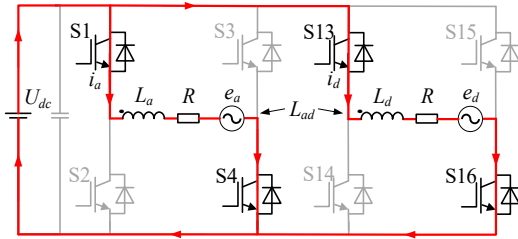


Fig. 11. Equivalent circuit of vertical-axis SPIM.

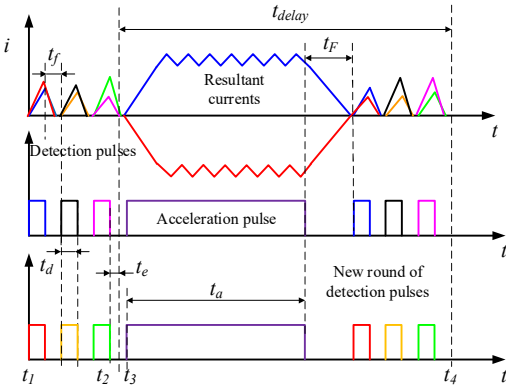


Fig. 12. Schematic diagram of vertical-axis SPIM.

In the period of three detection pulses, six-phase inductance information can be indirectly acquired.  $t_{delay}$  and  $\gamma$  can be optimized as (9) and (10), respectively.

$$t_{delay} = 3t_d + 2t_f + t_e + t_a + t_F \quad (9)$$

$$\gamma = \frac{t_a + t_F}{3t_d + 2t_f + t_e + t_a + t_F} \quad (10)$$

Fig. 13 shows the flowchart of vertical-axis SPIM. At the initial stage, vertical-axis synchronous pulses are injected, and the resultant currents are collected for comparison at the main intersection first. Once the sampled current is missing or out of reasonable range, assist intersection is introduced for position estimation. Then, acceleration pulses are injected to drive the machine.

As position-sensorless control methods are feasible for a specific speed region, once the rotor speed is larger than the threshold speed, the control mode should be switched to high-speed sensorless drive [15,16,27]. To ensure a smooth transition, two methods are chosen for their effectiveness in their respective speed ranges. The transition between the two sensorless methods occurs at a threshold speed where both methods work satisfactorily [31].

To achieve a smooth full-speed sensorless drive, the threshold should be selected at a certain level. Therefore, the detected signal such as back-EMF is large enough to be detected, thus guaranteeing the signal-to-noise ratio. To achieve more smooth transmission, the threshold speed selection often requires offline tuning by the trial-and-error methods [15,31].

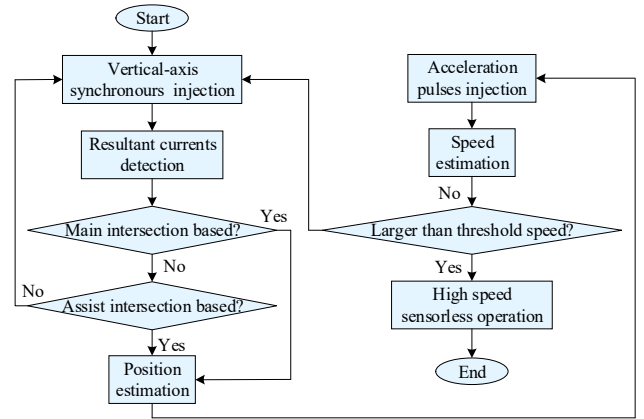


Fig. 13. Flowchart of vertical-axis SPIM.

### B. Analysis of Mutual Inductance Influence

As analyzed above, the mutual inductance coupling degree between vertical-axis phases is slight, and the range of fluctuations in the entire electrical angle period is small. When the detection pulses are injected into the vertical-axis phases A and D simultaneously, the equivalent circuit equation of phases A and D are shown in (11) and (12), respectively.

$$U_{dc} = i_a R + L_a \frac{di_a}{dt} + i_a \frac{dL_a}{d\theta} \omega + L_{ad} \frac{di_d}{dt} + i_d \frac{dL_{ad}}{d\theta} \omega \quad (11)$$

$$U_{dc} = i_d R + L_d \frac{di_d}{dt} + i_d \frac{dL_d}{d\theta} \omega + L_{ad} \frac{di_a}{dt} + i_a \frac{dL_{ad}}{d\theta} \omega \quad (12)$$

Insert (12) into (11), the formula can be simplified as

$$(L_a - L_{ad}) \frac{di_a}{dt} = (L_d - L_{ad}) \frac{di_d}{dt} \quad (13)$$

$$\frac{L_d - L_{ad}}{L_a - L_{ad}} = \frac{i_a}{i_d} \quad (14)$$

From the above analysis, due to the existence of mutual inductance, comparing  $I_a$  and  $I_d$  is comparing the magnitude relationship between  $L_a - L_{ad}$  and  $L_d - L_{ad}$  actually, which is equivalent to comparing  $L_a$  and  $L_d$ . By comparing the peak currents, the sector information can be deduced. Although the mutual inductance exists during the detection stage, this influence can be ignored.

### C. Analysis of Inductance Sampling Bias

A potential factor that affects sector estimation is inductance sampling bias caused by APIM. With the rotor rotation during the acceleration stage, the sampled phase inductance inevitably has a certain phase bias, rather than being sampled simultaneously. Therefore, sector estimation error may occur especially in the boundary sector. In APIM, the ideal inductance vectors of A, B, C, D, E and G and the detected inductance vectors of A', B', C', D', E' and G' are compared in Fig. 14(a). The phase bias between two adjacent phases vectors can be described as

$$\Delta\theta = \omega(t_d + t_f) \quad (15)$$

As the interval of detection phases increases, the detection phase bias will increase accordingly. Moreover, as  $\omega$  increases, the phase bias of detected inductance will increase accordingly. APIM is essentially to avoid the mutual inductance influence on self-inductance amplitudes detection, but these methods cause the phase bias in the inductance sampling in the acceleration stage. The inherent phase deviation of detected inductance can be avoided by vertical-axis SPIM fundamentally. As shown in Fig. 14(b), the three pairs of vertical-axis phases AD, BE and CG which compose main intersections, are detected without sample delay, thereby the accuracy of main intersection-base sector estimation can be guaranteed.

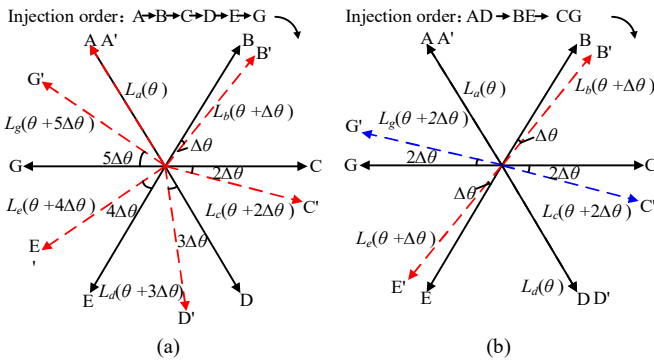


Fig. 14. Inductance vectors and sampling bias (a) APIM. (b) vertical-axis SPIM.

By the proposed method, full phases are detected within a half detection time. As a result,  $t_{delay}$  is decreased and  $\gamma$  is improved. It has been proved that the mutual inductance

influence on position estimation can be ignored, and no inductance sampling bias exists around the main intersections.

### D. Full Speed Sensorless Operation

Fig. 15 shows the full-speed sensorless control diagram. The resultant currents of vertical-axis detection pulses are collected for comparison through the sector estimator. In low-speed operation, the acceleration commands are generated as reference current excitation which contributes to torque generation. In this way, rotor speed can increase steadily. The current chopping regulator is applied in the current loop. Gate signals are sent to H-bridge converts directly. Once the speed reaches a certain level, the system can be switched to high-speed sensorless drive mode.

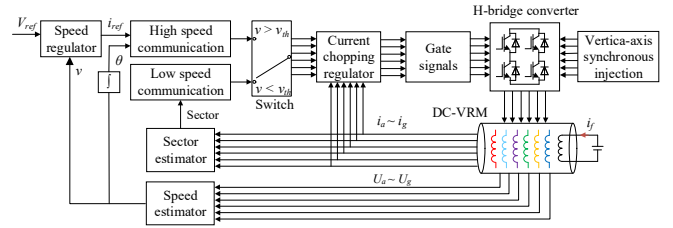


Fig. 15. Full speed control diagram.

## VI. PULSE INJECTION CLOSED COIL FAULTS DIAGNOSIS

In this research, six-phase DC-VRM is a kind of multiphase fault-tolerant machine, and its fault-tolerant capability is improved from parallel drive topology and sensorless drive method. On the one hand, the parallel drive topology allows each phase to be driven independently, so it has the inherent fault-tolerant ability when faced with an open-circuit fault. The faulty phase will not affect the healthy phase, which effectively reduces the impact of the open-circuit fault on the overall drive performance of the machine.

On the other hand, the redundant inductance intersections can provide the fault-tolerant ability of position estimation in the absence of current detection. Both full-phase APIM and vertical-axis SPIM can sample the whole phase currents, which means, a fault-tolerant threshold is provided when facing the current sampling fault. Reduce-APIM can be seen as a counter-evidence method that sacrifices part of the fault-tolerant ability to enhance acceleration performance.

For both open-circuit fault and current sensor damage, it is a common phenomenon that there is no current sensor signal in a faulty phase. How to distinguish these two faults is investigated, and a pulse injection closed coil fault diagnosis method by armature winding mutual inductance during the initial position detection stage is proposed. In this method, a closed coil is formed in a healthy phase by switching on related power transistors to detect the induced current excited by the faulty phase. As mutual inductance coupling exists between the armature windings, if the fault is caused by the damage of the current sensor, an induced current will be generated in the closed coil when a detection pulse is injected into the faulty phase. On the contrary, if the faulty phase suffers from an open



IEEE POWER ELECTRONICS REGULAR PAPER/LETTER/CORRESPONDENCE

circuit fault, no current can be detected in the healthy phase closed coil.

The equivalent circuit of pulse injection closed coil fault diagnosis is shown in Fig .16. For example, phase A suffers from a current sensor broken fault, and phase C is a healthy phase. By switching on transistors S10 and S12, a closed coil of phase C can be acquired, and a bidirectional induced current can pass through phase C to troubleshoot open circuit fault in phase A.

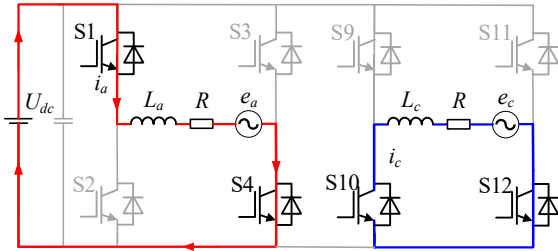


Fig. 16. Equivalent circuit of pulse injection closed coil fault diagnosis.

In addition, this method can also be used to locate the damaged transistor in an open circuit faulty phase. For example, phase A is a healthy phase, and phase C is an open circuit faulty phase but with a working current sensor. By injecting a detection pulse in phase A, if the negative current can be detected, the fault can be determined as the damage of the transistor 12. Therefore, the damaged transistor can be located, and the current sensor fault can be eliminated. Through this method, fault types can be distinguished exactly, and fault-tolerant operation methods for the two fault types are introduced.

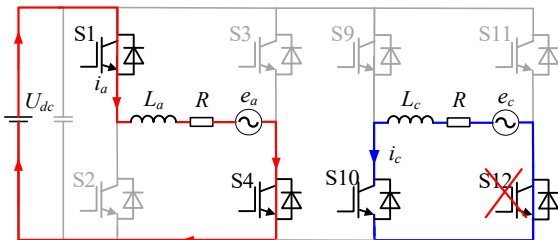


Fig. 17. Equivalent circuit of the pulse injection transistor fault diagnosis.

VII. EXPERIMENTAL RESULTS

In this chapter, full-phase APIM, reduced-phase APIM (four-phase APIM case 1) and vertical-axis SPIM are selected for further experimental analysis.

A. Experimental Setup

Experiments are carried out to verify the validity of the proposed pulse injection sensorless drive method. As the experimental setup is shown in Fig .18, the sensorless control is performed based on a real-time control platform of a dSPACE MicroLabBox with a simulation step size of 50us. Control parameters can be monitored by a personal computer or

oscilloscope. Commercial H-bridge converters are applied to drive the DC-VRM. The field winding is excited by the DC power source to establish the excitation magnetic field. A coaxial magnetic powder brake is connected to the DC-VRM. The actual rotor position is acquired by a resolver for reference.

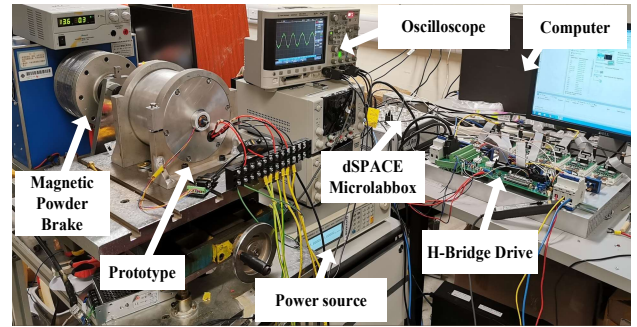


Fig. 18. Experimental setup.

B. Initial Position Detection

To acquire the initial position of the DC-VRM, detection pulses are injected into the armature windings, and then the resultant currents are compared to estimate the initial sector. Experiments of initial sector detection when the rotor is located in Sector VI are shown in Fig .19. all the pulse injection methods can estimate the initial sector precisely, thus guaranteeing the machine starts smoothly without reverse rotation.

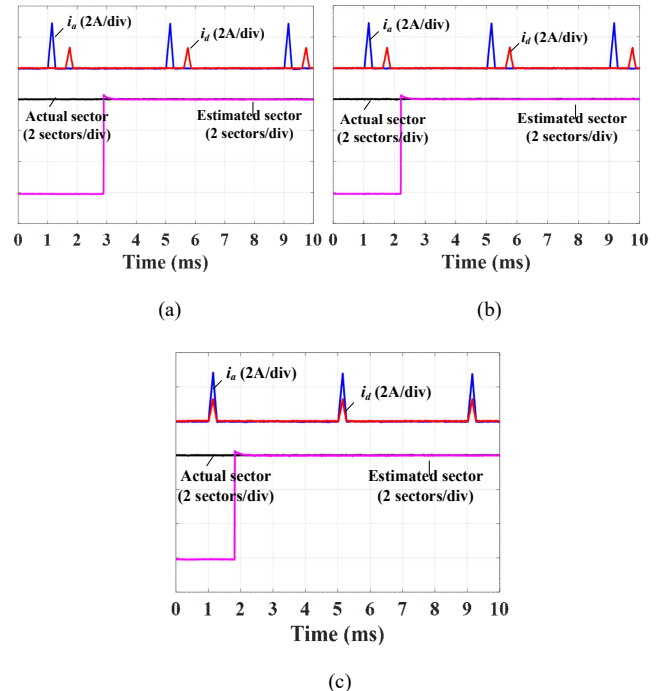


Fig. 19. Experiments of initial position detection. (a) Full-phase APIM. (b) Reduced-phase APIM. (c) Vertical-axis SPIM.

### C. Pulse Injection Closed Coil Faults Diagnosis

In the initial position detection stage, when the current sensor fails to detect the current, the proposed pulse injection closed coil faults diagnosis method can be applied. As shown in Fig. 19(a), by switching on power transistors S10 and S12, a closed coil is formed in the healthy phase C. Once the faulty phase A suffers from current sensor error without open circuit fault, an induced current is excited in the formed closed coil. Therefore, the open circuit fault can be excluded in phase A. Experimental results to locate a damaged power transistor in an open faulty circuit but with a working current sensor is shown in Fig. 20(b) and Fig. 20(c). The closed coil is formed by switching on power transistors S10 and S12. By injecting detection pulse in healthy phase A, if only one-directional current can be detected, the damaged power transistor can be located. The results are shown in Fig. 20(b) and Fig. 20(c) indicating the damaged power transistor are S10 and S12, respectively.

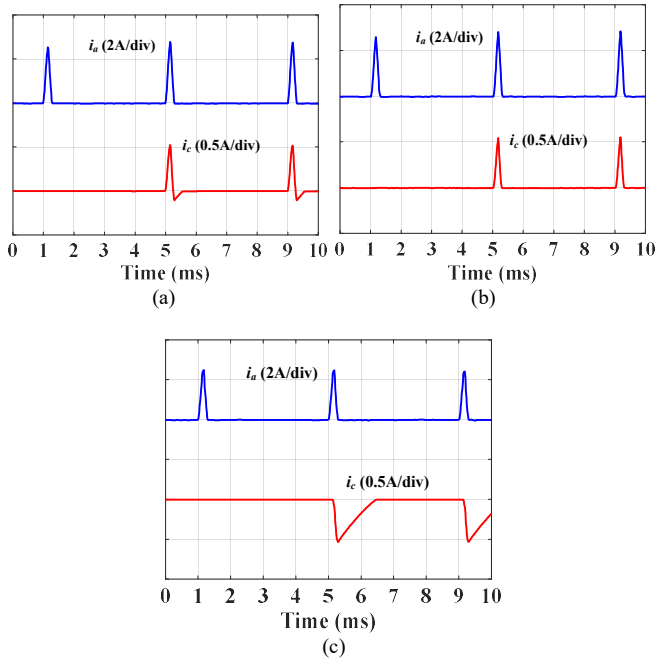


Fig. 20. Experiments of pulse injection closed coil fault diagnosis. (a) Current sensor fault. (b) Power transistor S10 fault. (c) Power transistor S12 fault.

### D. Sensorless Drive Acceleration

To further compare the impact of different pulse injection methods on acceleration performance, experiments are carried out.  $t_d$  and  $t_a$  are designed as 0.15ms and 1.25ms, respectively.  $t_f$  and  $t_r$  are reserved as 0.2ms and 1ms, respectively.  $t_e$  is decided by the sampling rate of the controller, which is 0.1ms. Load torque is 1Nm provided by magnetic powder brake. These parameters are kept all the same in the experiments, but only with different injection methods. As can be found in Fig. 21, all these methods can achieve sensorless start-up, but with quite different acceleration performances. Within one second of acceleration time, the full-phase APIM detection method can reach the speed of 100rpm, while the reduced-phase APIM can

reach the speed of 170rpm, both are lower than 220rpm acquired by the vertical-axis SPIM. The proposed vertical-axis SPIM can acquire a higher acceleration and a wider acceleration range in one second.

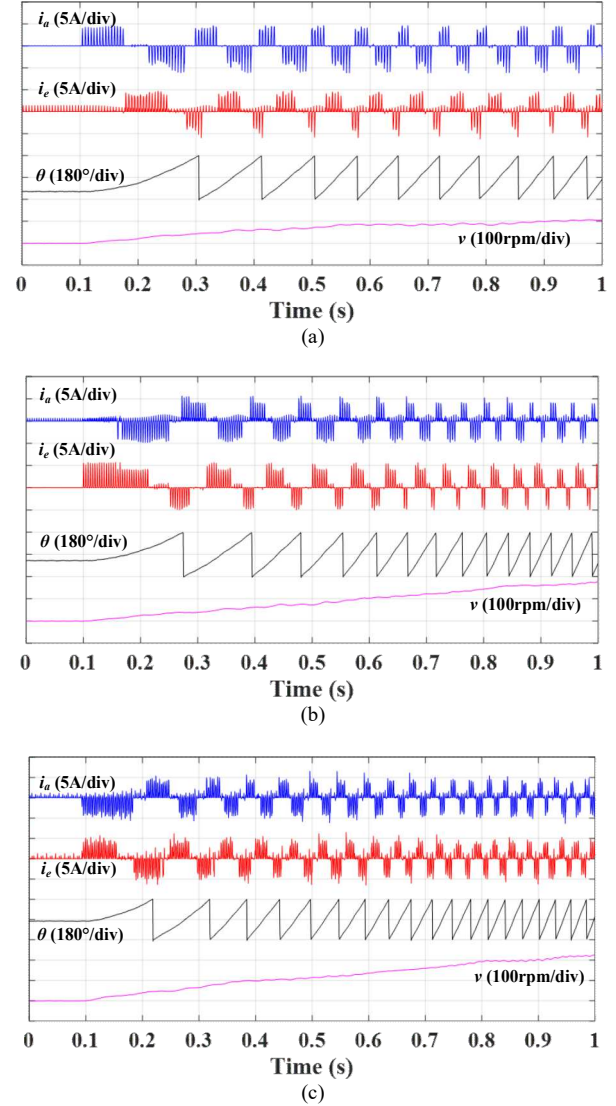


Fig. 21. Experimental results of acceleration. (a) Full-phase APIM. (b) Reduced-phase APIM. (c) Vertical-axis SPIM.

The performances of these three methods are compared in Table III. The proposed novel vertical-axis SPIM has both the merits of high acceleration performance and strong fault-tolerant ability.

TABLE III  
COMPARISON OF PULSE INJECTION METHODS

Detection methods	$t_{delay}$	$\gamma$	Fault-tolerant	Speed at 1s
Full-phase APIM	<4.35ms	51.7%	Strong	100rpm
Reduced-phase APIM	<3.65ms	61.6%	Weak	170rpm
Vertical-axis SPIM	<3.3ms	68.2%	Strong	220rpm

## IEEE POWER ELECTRONICS REGULAR PAPER/LETTER/CORRESPONDENCE

### VIII. DISCUSSION

In this study, pulse injection methods are optimized by minimizing the mutual inductance coupling between phases. The mutual inductance is mainly determined by the pole pair combinations, which also can be minimized by machine design. For example, the flux linkage is closed by a short magnetic circuit in 12/10 DC-VRM. Therefore, the flux passes through the adjacent phases, thus causing mutual inductance coupling between the armature windings. While for 12/8 DC-VRM, the flux linkage passes through its negative phase, thereby the mutual inductance between adjacent phases can be ignored. The discussion of this phenomenon can be found in [8]. Also, for DC-VRM, more pole pair combinations can be applied. As discussed in [9], for 12 slots design, 12/8 and 12/14 pole pair combinations have avoidable mutual inductance between armature windings. However, the torque ripple and cogging torque of these pole pair combinations are severe. Therefore, the design of the 12/10 pole pair combination is a better choice. And the mutual inductance influence can be minimized by the proposed vertical-axis SPIM.

It should be noticed that the proposed method is suitable for initial position estimation and acceleration. To achieve a full-speed sensorless drive and guarantee smooth transmission, the threshold speed selection requires offline tuning by the trial-and-error methods [15,31], more solid verifications will be conducted by combining novel high-speed sensorless drive methods in future research.

Some cost-saving drive topology can also be applied in DC-VRM sensorless drives. But their fault-tolerant ability is reduced compared with that of H-bridge converters. In this study, we focus on the research to achieve a solution to have a strong fault-tolerant ability for the potential aerospace applications. Therefore, a parallel H-bridge converter is a better solution. A specific analysis of cost-saving topology will be carried out in a future study.

### IX. CONCLUSION

This paper proposes a novel vertical-axis SPIM for six-phase DC-VRM to improve acceleration performance and guarantee fault-tolerant ability at the same time. First, the inductance characteristics, as well as their influence on sensorless control are analyzed. Then, the advantage of the multiphase machine in the sensorless drive is investigated as inductance intersections-based sector division that a smaller boundary sector can be acquired by main intersections, and fault-tolerant ability can be provided by assist intersections. Further, full-phase APIM is introduced to avoid mutual inductance on position estimation, and reduced-phase APIM is discussed in terms of acceleration performance and fault-tolerant ability. Finally, vertical-axis SPIM is proposed, and it has been proved that the mutual inductance influence on position estimation can be ignored, thereby high detection reliability and acceleration performance can be acquired without deterioration of fault-tolerant ability. Experimental results show that the proposed method has a high acceleration performance, and it can provide the fault-tolerant

ability for both current sampling fault and open circuit fault. Consequently, a solution that combines sensorless merits, low torque ripple and fault-tolerant ability can be achieved, which has good potential to be applied as an aero starter and generator.

### ACKNOWLEDGMENT

This work was supported by the National Natural Science Foundation of China under Project 52077187 and in part by the Research Grant Council of the Hong Kong Government under Project PolyU 152143/18E and PolyU 152109/20E.

### REFERENCES

- [1] J. Cao and A. Emadi, "A new battery/ultracapacitor hybrid energy storage system for electric, hybrid, and plug-in hybrid electric vehicles," *IEEE Trans. Power Electron.*, vol. 27, no. 1, pp. 122-132, Jan. 2012.
- [2] K. T. Chau, C. C. Chan and C. Liu, "Overview of permanent-magnet brushless drives for electric and hybrid electric vehicles," *IEEE Trans. Ind. Electron.*, vol. 55, no. 6, pp. 2246-2257, June 2008.
- [3] I. Boldea, L. N. Tutelea, and D. Dorrell, "Automotive electric propulsion systems with reduced or no permanent magnets: an overview," *IEEE Trans. Ind. Electron.*, vol. 61, no. 10, pp. 5696-5711, Oct. 2014.
- [4] X. Zhao, S. Niu, and W. Fu, "Design of a new relieving-DC-saturation hybrid reluctance machine for fault-tolerant in-wheel direct drive," *IEEE Trans. Ind. Electron.*, vol. 67, no. 11, pp. 9571-9581, Nov. 2020.
- [5] Y. Jin, B. Bilgin, and A. Emadi, "An extended-speed low-ripple torque control of switched reluctance motor drives," *IEEE Trans. Power Electron.*, vol. 30, pp. 1457-1470, 2015.
- [6] Z. Chen, and Y. Yan "A doubly salient starter/generator with two section twisted-rotor structure for potential future aerospace application," *IEEE Trans. Ind. Electron.*, vol. 59, no. 9, pp. 3588- 3595, Sept. 2012.
- [7] L. R. Huang, J. H. Feng, S. Y. Guo, J. X. Shi, W. Q. Chu and Z. Q. Zhu, "Analysis of torque production in variable flux reluctance machines," in *IEEE Trans. Energy Convers.*, vol. 32, no. 4, pp. 1297-1308, Dec. 2017.
- [8] S. Jia, R. Qu, J. Li, D. Li and H. Lu, "Design considerations of stator DC-winding excited vernier reluctance machines based on the magnetic gear effect," *IEEE Trans. Ind. Appl.*, vol. 53, no. 2, pp. 1028-1037, March-April 2017.
- [9] X. Liu and Z. Q. Zhu, "Stator rotor pole combinations and winding configurations of variable flux reluctance machines," *IEEE Trans. Ind. Appl.*, vol. 50, no. 6, pp. 3675-3684, Nov.-Dec. 2014.
- [10] X. Zhao and S. Niu, "Design and optimization of a novel slot-PM-assisted variable flux reluctance generator for hybrid electric vehicles," *IEEE Trans. Energy Convers.*, vol. 33, no. 4, pp. 2102-2111, Dec. 2018.
- [11] T. Dos Santos Moraes, N. K. Nguyen, E. Semail, F. Meinguet and M. Guerin, "Dual-Multiphase Motor Drives for Fault-Tolerant Applications: Power Electronic Structures and Control Strategies," *IEEE Trans. Power Electron.*, vol. 33, no. 1, pp. 572-580, Jan. 2018.
- [12] I. Gonzalez-Prieto, M. J. Duran, F. Barrero, M. Bermudez and H. Guzmán, "Impact of Postfault Flux Adaptation on Six-Phase Induction Motor Drives with Parallel Converters," *IEEE Trans. Power Electron.*, vol. 32, no. 1, pp. 515-528, Jan. 2017.
- [13] F. Genduso, R. Miceli, C. Rando and G. R. Galluzzo, "Back EMF Sensorless-Control Algorithm for High-Dynamic Performance PMSM," *IEEE Trans. Ind. Electron.*, vol. 57, no. 6, pp. 2092-2100, June 2010.
- [14] G. Wang, M. Valla and J. Solsona, "Position Sensorless Permanent Magnet Synchronous Machine Drives—A Review," *IEEE Trans. Ind. Electron.*, vol. 67, no. 7, pp. 5830-5842, July 2020.
- [15] E. Ofori, T. Husain, Y. Sozer and I. Husain, "A Pulse-Injection-Based Sensorless Position Estimation Method for a Switched Reluctance Machine Over a Wide Speed Range," *IEEE Trans. Ind. Appl.*, vol. 51, no. 5, pp. 3867-3876, Sept.-Oct. 2015.
- [16] D. Xiao, J. Ye, G. Fang, Z. Xia, X. Wang and A. Emadi, "Improved Feature-Position-Based Sensorless Control Scheme for SRM Drives Based on Nonlinear State Observer at Medium and High Speeds," *IEEE Trans. Power Electron.*, vol. 36, no. 5, pp. 5711-5723, May 2021.

IEEE POWER ELECTRONICS REGULAR PAPER/LETTER/CORRESPONDENCE

- [17] M. Ehsani, I. Husain and A. B. Kulkarni, "Elimination of discrete position sensor and current sensor in switched reluctance motor drives," *IEEE Trans. Ind. Appl.*, vol. 28, no. 1, pp. 128-135, Jan.-Feb. 1992.
- [18] M. Ehsani, I. Husain, S. Mahajan and K. R. Ramani, "New modulation encoding techniques for indirect rotor position sensing in switched reluctance motors," *IEEE Trans. Ind. Appl.*, vol. 30, no. 1, pp. 85-91, Jan.-Feb. 1994.
- [19] J. Cai, Z. Liu, Y. Zeng, H. Jia and Z. Deng, "A Hybrid-Harmonic-Filter-Based Position Estimation Method for an SRM with Embedded Inductive Sensing Coils," *IEEE Trans. Power Electron.*, vol. 33, no. 12, pp. 10602-10610, Dec. 2018.
- [20] S. M. Ahmed and P. W. Lefley, "A new simplified sensorless control method for a single-phase SR motor using HF signal injection," in *Proc. IEEE Univ. Power Eng. Conf.*, 2007, pp. 1075-1078.
- [21] J. Ye, B. Bilgin and A. Emadi, "Elimination of Mutual Flux Effect on Rotor Position Estimation of Switched Reluctance Motor Drives," *IEEE Trans. Power Electron.*, vol. 30, no. 3, pp. 1499-1512, March 2015.
- [22] J. Cai and Z. Liu, "An Unsaturated Inductance Reconstruction Based Universal Sensorless Starting Control Scheme for SRM Drives," *IEEE Trans. Ind. Electron.*, vol. 67, no. 11, pp. 9083-9092, Nov. 2020.
- [23] Hongwei Gao, F. R. Salmasi and M. Ehsani, "Inductance model-based sensorless control of the switched reluctance motor drive at low speed," *IEEE Trans. Power Electron.*, vol. 19, no. 6, pp. 1568-1573, Nov. 2004.
- [24] M. Krishnamurthy, C. S. Edrington and B. Fahimi, "Prediction of rotor position at standstill and rotating shaft conditions in switched reluctance machines," *IEEE Trans. Power Electron.*, vol. 21, no. 1, pp. 225-233, Jan. 2006.
- [25] G. Pasquosoone, R. Mikail and I. Husain, "Position Estimation at Starting and Lower Speed in Three-Phase Switched Reluctance Machines Using Pulse Injection and Two Thresholds," *IEEE Trans. Ind. Appl.*, vol. 47, no. 4, pp. 1724-1731, July-Aug. 2011.
- [26] J. Cai and Z. Deng, "Sensorless Control of Switched Reluctance Motor Based on Phase Inductance Vectors," *IEEE Trans. Power Electron.*, 27, no. 7, pp. 3410-3423, July 2012.
- [27] Y. Zhao, H. Wang, H. Zhang and L. Xiao, "Position-Sensorless Control of DC + AC Stator Fed Doubly Salient Electromagnetic Motor Covered Full Speed Range," *IEEE Trans. Ind. Electron.*, vol. 62, no. 12, pp. 7412-7423, Dec. 2015.
- [28] X. Zhou and B. Zhou, "Rotor position estimating scheme for doubly salient EM machine sensorless startup," *IET Electron. Lett.*, vol. 53, no. 15, pp. 1033-1044, Jul. 2017.
- [29] X. Zhou, B. Zhou and J. Wei, "A Novel Position-Sensorless Startup Method for DSEMI *IEEE Trans. Ind. Appl.*, vol. 54, no. 6, pp. 6101-6109, Nov.-Dec. 2018.
- [30] X. Zhou, B. Zhou, K. Wang, L. Zhang and Y. Zhao, "Two-Step Rotor Position Estimation Method for Doubly Salient Electromagnetic Starter-Generator Over Zero and Low Speeds Range," *IEEE J. Emerg. Sel. Topics Power Electron.*, vol. 9, no. 3, pp. 2664-2673, June 2021.
- [31] A. Khalil *et al.*, "Four-Quadrant Pulse Injection and Sliding-Mode-Observer-Based Sensorless Operation of a Switched Reluctance Machine Over Entire Speed Range Including Zero Speed," *IEEE Trans. Ind. Appl.*, vol. 43, no. 3, pp. 714-723, May-june 2007.



**WEIYU WANG** is currently working toward the Ph.D. degree in electrical engineering with the Department of Electrical Engineering, Hong Kong Polytechnic University, Hong Kong, China. His research interests include electrical machine drive and position-sensorless drive.



**XING ZHAO** (Member, IEEE) received the B.Eng. degree from Nanjing University of Aeronautics and Astronautics, Nanjing, China, in 2014, and the Ph.D. degree from The Hong Kong Polytechnic University, Hong Kong, China, in 2020, both in Electrical Engineering.

From Jul. 2019 to Jan. 2020, he was a Visiting Research Scholar with the Center for Advanced Power Systems, Florida State University, Tallahassee, USA. Between Jul. 2020 and Oct. 2021, he served as a Research Assistant Professor with the Department of Electrical Engineering, The Hong Kong Polytechnic University. Since Nov. 2021, he has been a Lecturer in the Department of Electronic Engineering with University of York, UK. He has authored or coauthored more than 50 technical papers in the international journals and conferences and holds six granted patents. His research interests include advanced electrical machines, motor drives, and power electronics for electric vehicles and renewable energy systems.



**SHUANGXIA NIU** (Senior Member, IEEE) received the B.Sc. and M.Sc. degrees in electrical engineering from the School of Electrical Engineering and Automation, Tianjin University, Tianjin, China, in 2002 and 2005, respectively, and the Ph.D. degree in electrical engineering from the Department of Electrical and Electronic Engineering, The University of Hong Kong, Hong Kong, in 2009, all in electrical engineering.

Since 2009, she has been with The Hong Kong Polytechnic University, Hong Kong, where she is currently an Associate Professor with the Department of Electrical Engineering. She has authored or coauthored over 100 articles in leading journals. Her research interests include novel electrical machines and drives, renewable energy conversion systems, and applied electromagnetics.



**WEINONG FU** obtained his PhD from The Hong Kong Polytechnic University (PolyU) in 1999. He is a Professor at Shenzhen Institutes of Advanced Technology, Chinese Academy of Sciences. He worked at PolyU about 13 years as an Associate Professor and full Professor. He was one of the key developers at Ansoft Corporation in Pittsburgh, USA. He has about seven years of working experience at Ansoft, focusing on the development of commercial software Maxwell®, which is a leading commercial software package for the computation of electromagnetic fields of electromechanical equipments. During 1982 to 1986, he worked at *Shanghai Electrical Apparatus Research Institute*,

#### IEEE POWER ELECTRONICS REGULAR PAPER/LETTER/CORRESPONDENCE

where he accumulated valuable experience to deal with the design and manufacturing of electric devices in practice, and constructed a solid foundation for further academic career development. Prof. Fu has made many contributions to the theory and application of electromagnetic field computation and electric device design, including the publication of over 250 refereed journal papers. He regularly serves as paper reviewer

for *IEEE Trans. Magnetics*, *IEEE Trans. Energy Conversion*, *IEEE Trans. Industrial Electronics*, *IEEE Trans. Power Electronics*, *IEEE Trans. Industry Application*, *Energies*, and *COMPUMAG*, *CEFC*, *INTERMAG* international conferences. Prof. Fu's research interests mainly focus on computational electromagnetics, optimal design of electric devices, applied electromagnetics, and novel electric machines.